Journal of Structural Geology 33 (2011) 62–77

Contents lists available at ScienceDirect

Journal of Structural Geology

journal homepage: www.elsevier.com/locate/jsg

Structural evolution of fold-thrust structures in analog models deformed in a large geotechnical centrifuge

Todd E. Noble*, John M. Dixon

Experimental Tectonics Laboratory, Department of Geological Sciences, Queen's University, Kingston, Ontario, Canada K7L 3N6

ARTICLE INFO

Article history:
Received 7 May 2010
Received in revised form
11 December 2010
Accepted 13 December 2010
Available online 21 December 2010

Keywords:
Analogue experiments
Centrifuge modeling
Fault-propagation folding
Distance-displacement methods
Thrust sheet deformation

ABSTRACT

We investigate the structural evolution of fault-propagation folds and fold-thrust systems with scaled analog modeling carried out using the 5.5 m radius geotechnical centrifuge at C-CORE, St. John's NL. The experiments presented here are the first of their kind, scaled ten times larger than predecessors and deformed using a custom rig with load monitoring and displacement control. Plane-layered models approximately 1 m long and representing 50 km sections are shortened horizontally under an enhanced gravity field of 160 g. The large model scale allows for a proportionally large number of bedding laminations that act as strain markers. This allows detailed analysis of strain partitioning and interplay, both at the scale of a fold-thrust system and the individual fold-thrust structure. Layer-parallel shortening ("LPS") and rotation of fault-bounded blocks are revealed by mapping contraction fault populations and bedding-contraction fault intersection angles. Low-angle contraction faulting and LPS are found to be dominant at early stages of development and rotation of fault-bounded blocks occurs during progressive folding of the hanging-wall panel during fault-propagation folding. Displacement-distance data obtained from major thrusts in the model show relative stretch values, and consequently fault slip/propagation ratios, that are similar to natural structures.

1. Introduction

Reconstructing a complete multi-scale strain history of a natural fold-thrust structure based on field observations of macroscopic deformation features and microscopic fabric elements is challenging. The deformation processes of folding, faulting and penetrative deformation are competing strain accommodation mechanisms, all of which are active in varying proportions throughout the evolution of a fold-thrust structure (Jamison, 1992; Woodward, 1999). The scale of the observation is also important; for example, penetrative strain in a thrust sheet can be viewed either as a ductile process at the regional scale or brittle deformation at the hand-sample and thin-section scale (Price, 1973). Re-construction of a strain history therefore requires both an understanding of the relationship and interaction of the macroscopic folding and faulting processes, and the mesoscopic and microscopic fabric-forming processes.

Field observations of the interaction of folding and thrusting (Willis and Willis, 1934; Dahlstrom, 1970; Williams and Chapman, 1983) have been used to develop geometric and kinematic models for detachment and fault-propagation folding, structural styles which are characterized by different types of interaction between folding and faulting (e.g. Suppe, 1983; Jamison, 1987; Suppe and Medwedeff, 1990). Mechanisms such as brittle fracturing and penetrative deformation accommodate internal strain during the deformation and transport of thrust sheets (e.g. Reks and Gray, 1983; Wojtal, 1986; Geiser, 1988). Meso- and microscopic features such as faults, fractures, cleavage and stylolites constitute fabric elements that are useful for reconstructing strain history (e.g. Woodward et al., 1986). Overprinting and cross-cutting of structural elements observed at outcrop, hand-sample and microscopic scales suggest that the strain distribution has evolved within the rocks according to the local passage of propagating fault tips, fold growth and thrust sheet transport (Dahlstrom, 1970; McConnell et al., 1997; Nicol et al., 2002; Price, 1967). Furthermore, field studies suggest that thrust sheet strain varies systematically between frontal and lateral ramps, as a function of thrust propagation and internal strain mechanisms specific to their geometries (Coward and Potts, 1983; Wibberley, 1997). In this context, dislocated folds can be interpreted as remnants of the propagation stage of a thrust fault now carried passively or modified by subsequent thrust sheet strains. Earlier strain events related to the incipient propagation of fault tips and the low-strain "process zone" deformation (Cowie and Scholz, 1992; Jolley et al., 2004) are rarely preserved, and are difficult to deconvolve from subsequent strain

* Corresponding author. Present address: Shell Canada Ltd., 400 4th Avenue SW, P.O. Box 100, Station M, Calgary, Alberta, Canada T2P 2H5. Tel.: +1 403 691 3251.
E-mail addresses: Todd.Noble@Shell.com (T.E. Noble), John.Dixon@queensu.ca (J.M. Dixon).

0191-8141/$ – see front matter © 2010 Elsevier Ltd. All rights reserved.
doi:10.1016/j.jsg.2010.12.007

events that are imparted on the rocks. Subsequent phases of deformation can be imparted on thrust sheets through a normal sequence of thrust development, with younger thrusts tending to form beneath and on the foreland side of older ones. The resulting older fold-thrust structures tend to be subjected to deformation as they are carried up ramps on the underlying younger thrusts.

Since geological structures evolve on a time-scale too large for direct observation, a high-resolution forward modeling method is needed that captures incipient strain patterns and clearly demonstrates the evolution and interplay between strain mechanisms at different scales. Ideally, modeling enables prediction and explanation of strain type, intensity and distribution for fold-thrust structures that are comparable to field outcrop examples.

Physical analog modeling is a proven tool for understanding the interplay of folding, thrusting and penetrative strain. Pioneering work by Davis et al. (1983) and Malavieille (1984) laid the foundation of modeling fold-thrust structures with simple sandbox models. Peltzer (1988) used a large geotechnical centrifuge to conduct experiments investigating the large-scale tectonics of the India–Eurasia collision. Dixon and Liu (1992) and Liu and Dixon (1995) used the centrifuge technique of modeling with layered visco-plastic materials to demonstrate localization of thrust ramps by buckle folding; Storti et al. (1997) studied the nucleation and displacement profiles of thrust fault-related folds in sandbox models with layered granular materials; and Adam et al. (2005) introduced high-resolution optical correlation techniques to monitor displacement fields in order to quantify the spatial and temporal patterns of strain accumulation, including folding, faulting and penetrative strain. A short-coming of sandbox models that use granular materials is the model stratigraphic sequences typically fail to simulate the inherent bedding anisotropy of natural stratified sedimentary rocks. Some degree of anisotropy has been added to sandbox modeling by introducing materials with different mechanical properties (Colletta et al., 1991; Teixell and Koyi, 2003). In addition, the granular materials in sandbox models do not typically reveal the small-scale brittle deformation features that contribute to the overall internal strain picture. Plasticine and silicone putty analog models also have their limitations: they tend to deform in ductile folding styles typical of structures in the middle to deep crust; the adhered nature of the layers tends to inhibit interlayer slip widely observed in natural structures; and surface processes like erosion and sedimentation are difficult to include in the modeling process.

This paper presents experimental results of dynamically scaled analog models constructed of stiff visco-plastic materials that are deformed in a large (5.5 m radius) geotechnical centrifuge. These models are based on smaller-scale equivalents deformed in a (30 cm radius) centrifuge at the Experimental Tectonic Laboratory at Queen's University (Dixon and Liu, 1992; Liu and Dixon, 1990, 1991, 1995). This analog modeling technique enables observation of the structural evolution of fold-thrust structures, including fold-thrust relationships and the development of deformation fabrics. With their large size, the models are constructed with a large number of thin, mechanically passive laminae "bedding" which act as strain markers. The strain markers record mesoscopic deformation fabrics that reveal where and when strain accommodation mechanisms are active within fold-thrust structures. Also, these markers record the evolution of fold-thrust relationships during the deformation, and allow a comparison to geometrical and kinematic models previously derived from natural analog structures. We demonstrate that these models are scaled representations of earlier centrifuge experiments as well as natural prototype systems; passive bedding laminae reveal complex strain accommodation mechanisms and fold-thrust relationships unseen in previous centrifuge models; and model fold-thrust relationships are consistent with published folding and fault-propagation concepts formed from observation of natural structures.

2. Experimental setup and procedure

2.1. Modeling apparatus

The experimental work reported here was carried out at the C-CORE facility in St. John's, NL, Canada that houses an Accutronic 680-2 centrifuge (Fig. 1). This machine can accommodate a payload package measuring up to 1.1 m (h) by 1.4 m (l) by 1.1 m (w), with a load capacity of 130 g-tonnes at a maximum acceleration of 200 g that is attained at 189 RPM. The platform also contains an onboard data-acquisition system to record real-time measurements from the test package while the platform is in flight.

A custom experiment package was designed and built for this project. The model is contained within a rectangular aluminum box measuring 100 cm long, 10 cm wide and 10 cm high. A mechanical drive system advances a loading platen that shortens the model in the "model horizontal" direction. The loading platen is fixed beneath a trolley that rides on overhead rails and is pulled toward the foreland end of the model by aircraft cables collected on a spool driven by a servo-motor (Fig. 2a and b). The model container, drive system and instrumentation are completely enclosed in a strongbox for protection in the event of catastrophic failure during flight.

Onboard instrumentation allows the position of the loading platen to be accurately monitored, and experiments can be conducted at either a constant displacement rate or a constant-load setting. In controlled displacement rate experiments the platen is advanced at a programmed speed selected to scale the average model shortening rate to that of the prototype system and consistent with other model scale ratios chosen so that the model materials behave most like their natural counterparts (Dixon and Summers, 1985).

The loading platen is also equipped with load-measuring devices, including a tension load cell connected to the pulling cables, and compressional load cells positioned on the loading platen. Additional compressional load cells mounted within the free-standing loading plate are in direct contact with the end of the model to measure the local stress at different heights on the hinterland end. This setup allows the applied load to be monitored during constant displacement rate experiments, or the shortening rate to be adjusted with a feed-back loop during constant-load experiments.

The study reported here involved experiments conducted at a constant displacement rate and herein we do not discuss the load data collected.

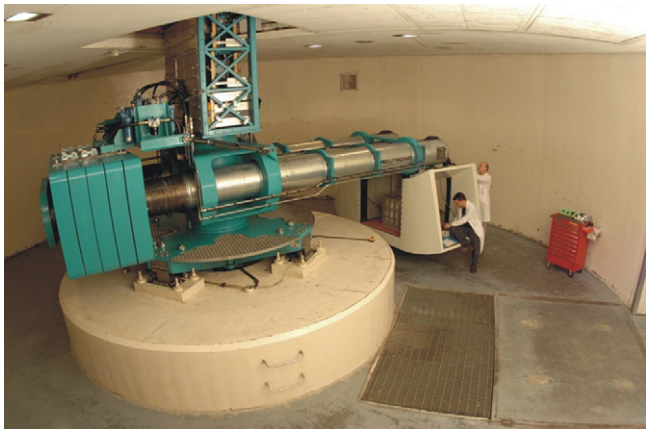

Fig. 1. The C-CORE Accutronic 680-2 centrifuge.

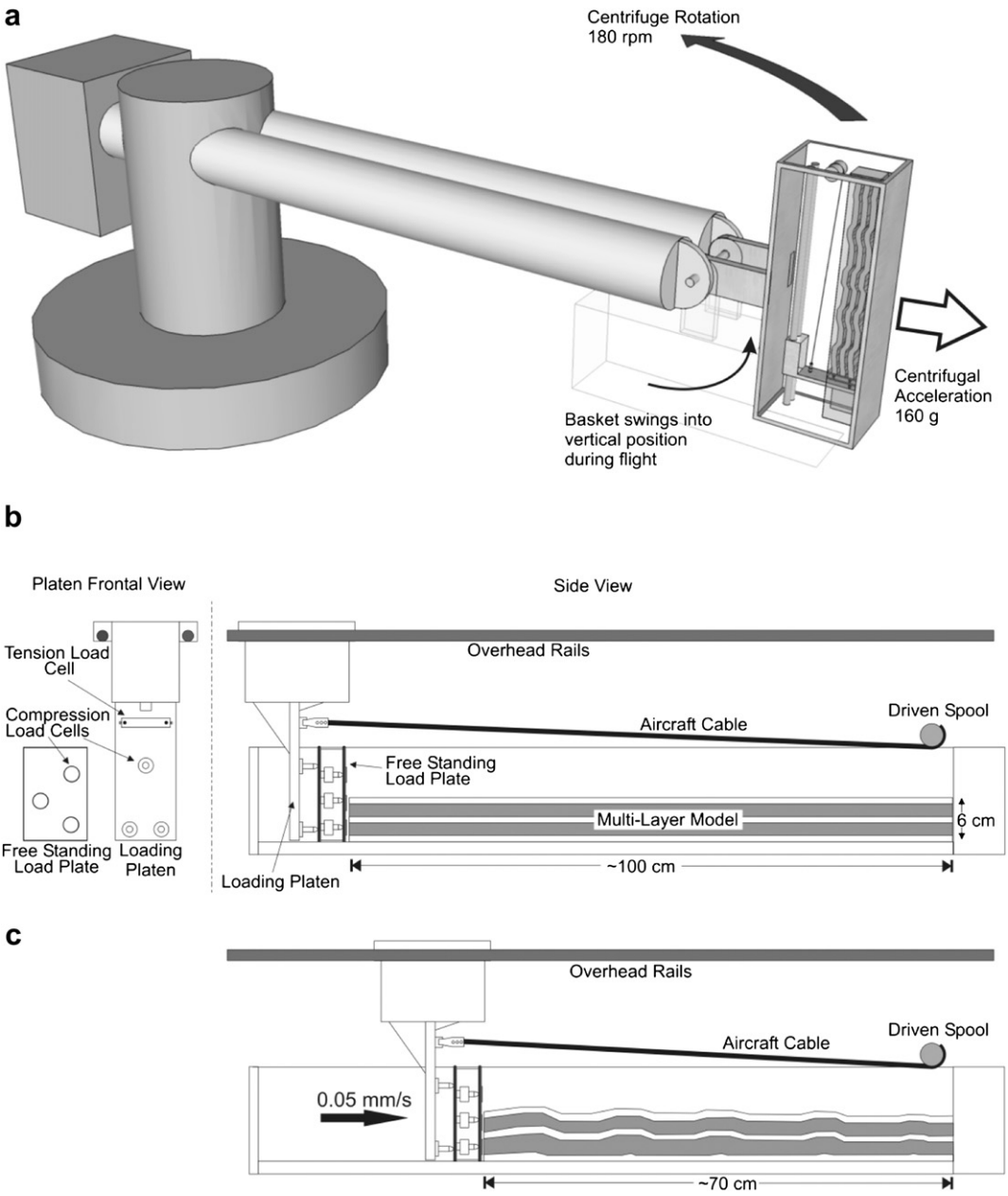

Fig. 2. Schematic diagram of the C-CORE centrifuge (a) showing the resting and in flight basket orientations. Schematic profiles of the test package used for shortening models: (b) at onset (c) after the model is subjected to 30% bulk shortening.

The models are constructed of Plasticine™ modeling clay (Harbutts Gold Medal Brand "plasticine") and silicone putty (Dow Corning Dilatant Compound 3179). Competent stratigraphic units are composed of layered plasticine, and are mechanical analogs for limestones or coarse clastic rocks. Rheological testing of plasticine by McClay (1976) found that plasticine deforms plastically in pure shear tests with strain rates between 10^{-3} s^{-1} and 10^{-6} s^{-1}, as a non-linear, strain-rate softening, but strain hardening material. Incompetent units are composed of alternating silicone putty and plasticine layers that represent shale interbedded with sandstone, limestone or siltstone (Dixon and Summers, 1986). Silicone putty is the weaker of the two materials and when deformed under strain rates between 10^{-5} s^{-1} and 10^{-3} s^{-1}, deforms by inelastic and non-recoverable ductile strain that is best approximated by power-law creep behavior with $n = 7 \pm 2$ (Dixon and Summers, 1985). A unit comprising inter-layered silicone putty and plasticine has both reduced bulk competency as well as pronounced planar anisotropy simulating sedimentary bedding, in comparison to a unit comprised only of plasticine.

Dixon and Summers (1985) described the method of preparing internally laminated units comprising alternating laminae of plasticine and silicone putty. To construct stratigraphic units for small-sized models for experiments in the Queen's University centrifuge, the materials can be rolled by hand with a steel roller and guide bars of various thicknesses. However, the construction of the larger models described here required the use of an electrically powered mechanical device known as a "reversible sheeter". This device is normally used for rolling dough in commercial bakeries. The reversible sheeter prepares sheets of the model materials by passing the material forwards and backwards on a conveyor belt between vertically aligned steel rollers. The roller separation is progressively decreased after each successive pass to reduce the thickness of the layer of material. The thinned units can then be cut

and stacked to double the number of layers, and then thinned again. Model units can be constructed that contain either alternating colors of plasticine or alternating layers of plasticine and silicone putty. The rolling and stacking process can be repeated until the desired number of laminae and the desired unit thickness is achieved, with laminae as thin as 0.1 mm. At a length scaling ratio of 20 mm = 1 km, this represents a prototype bed thicknesses of approximately 5 m which is well suited to represent natural interbedded units. Models can be built to represent a variety of stratigraphic sequences by stacking individual mechanical units with different internal laminations. For example, a unit representing competent carbonate would consist of alternating laminae of plasticine of different colors, and a unit representing interbedded shale/limestone would consist of inter-layered silicone putty and plasticine.

After construction a model is placed in the aluminum box. The sides of the model are lubricated with petroleum jelly to reduce the friction between the model and the aluminum side-walls during deformation. The experimental package is placed within the protective strongbox and mounted into the swinging payload platform of the centrifuge. Once in flight, the test platform swings outward until it is oriented perpendicular to the centrifuge arm and the long dimension of the model is oriented vertically, parallel to the axis of rotation (Fig. 2a). The test platform achieves complete perpendicularity at approximately 10 g, well before the experimental conditions of 160 g for these experiments. The motor drive system in the test package is then engaged and the model is shortened to the desired extent. The experiment can be run in stages so that the evolution of structures can be monitored.

2.2. Analog materials and model scaling

Physical scale modeling at both the Queen's University Experimental Tectonics Lab and C-CORE follow scale model theory, as outlined by Hubbert (1937) and Ramberg (1967), to ensure that the selected set of length, density, time (strain-rate) and acceleration ratios lead to the development of realistic representations of geologic structures.

The models deformed at Queen's University were limited by the length of the smaller payload box, and necessitated a model ratio of length typically about 10^{-6} (1 mm = 1 km). Other key model ratios are fixed by the prototype and model materials as shown in Table 1. With these ratios fixed, a suitable acceleration ratio (**g**-level for the centrifuge experiment) is selected to achieve accurate scaling of stresses between the model and the natural prototype, typically 3200 **g**.

Model experiments conducted in the C-CORE centrifuge use the same materials as experiments performed at Queen's University and thus have similar ratios for density and viscosity (Table 1). C-CORE models are typically 20 times thicker (vertical dimension) than the models deformed at Queen's University, and have a length scaling ratio of approximately 2×10^{-5} (20 mm = 1 km). C-CORE experiments are conducted with an acceleration ratio of 1.6×10^{2}, or 1/20th of the acceleration ratio for an equivalent experiment at Queen's University. Selecting these length and acceleration ratios produces similar model stress ratios for C-CORE and experiments at Queen's University. The Ramberg number is calculated as the ratio of gravitational forces to viscous forces for an experiment and represents a measure of dynamic similarity between the model and prototype (Ramberg, 1981; Weijermans and Schmeling, 1986). The Ramberg number for experiments at Queen's University, C-CORE and the equivalent natural prototype are within an order of magnitude and can be considered to be in close agreement (Table 1) (Koyi, 1988). By maintaining a similar stress ratio and equivalent Ramberg numbers, experiments at C-CORE and Queen's University should evolve in a dynamically, kinematically and geometrically similar fashion to each other and to the natural prototype.

3. Structural evolution and strain partitioning of model fold-thrust systems

Two models deformed in the C-CORE centrifuge demonstrate this analog modeling technique. They were based on the TH20-24 series of models deformed in the centrifuge at Queen's University (Fig. 3) (Liu and Dixon, 1990, 1991). The models deformed at Queen's University are composed of six internally laminated stratigraphic units of alternating bulk competency with an incompetent unit at the base, and they developed geologically realistic fold-thrust structures. In comparison, C-CORE models TN16 and TN17 were constructed of five layered stratigraphic units of alternating bulk competency, with an incompetent unit at the base (Fig. 4). TN16 and TN17 differed in that the middle incompetent unit III was thinner by 2 mm, or 100 m at prototype dimensions, in TN17. This thickness difference in unit III might be expected to create differences in the individual modeling results. Compared to the Queen's models, the TN models maintained the proportional thickness of the competent beams relative to the incompetent units as well as the thickness of individual laminae in each unit (Table 2).

3.1. Structural evolution of a model fold-thrust system

Models TN16 and TN17 were horizontally shortened in two stages to allow photographing mid-way through the experiment. The experiment details are summarized in Table 3.

During the first stage a buckle fold train developed serially in the competent units with the folds diminishing in amplitude toward the foreland (Figs. 5a and 6a). The buckle fold structures in the lower competent beam are labeled in order of sequential nucleation from hinterland to foreland as structures S_1 through S_5. During

Table 1
Scaling ratios of models deformed at Queen's Experimental Tectonic Laboratory and the C-CORE centrifuge center.

Quantity	Queen's University models	C-CORE models	Equivalence for C-CORE models
Length Ratio	$l_r = 1.0 \times 10^{-6}$	$l_r = 2.0 \times 10^{-5}$	20 mm ≡ 1 km
Specific Gravity Ratio	$\rho_r = 0.6$	$\rho_r = 0.6$	1.60 ≡ 2.67 (average bulk value for the whole stratigraphic column)
Time Ratio (strain-rate)	$t_r = 1.0 \times 10^{-11}$	$t_r = 1.0 \times 10^{-11}$	e.g. 10^{-4} s^{-1} ≡ 10^{-15} s^{-1}
Viscosity Ratio	$\mu_r = 2.4 \times 10^{-14}$	$\mu_r = 2.4 \times 10^{-14}$	2.4×10^{2} Pa s ≡ 10^{16} Pa s
Acceleration Ratio	$a_r = 3.2 \times 10^{3}$	$a_r = 1.6 \times 10^{2}$	160 **g** ≡ 1 **g**
Stress Ratio	$\sigma_r = \rho_r \cdot l_r \cdot a_r = 1.9 \times 10^{-3}$	$\sigma_r = \rho_r \cdot l_r \cdot a_r = 1.9 \times 10^{-3}$	(calculated from other ratios)
Ramberg Number	$R_m = \frac{g \cdot l^2 \cdot \rho}{\mu \cdot v} = 2.4 \times 10^{6}$ [a]	$R_m = \frac{g \cdot l^2 \cdot \rho}{\mu \cdot v} = 1.7 \times 10^{7}$ [b]	$1.7 \times 10^{7} \equiv 3.5 \times 10^{7}$ [c]

[a] The characteristic velocity (v) for Queen's University experiment is 5×10^{-5} m/s with a gravity (g) of 3200 g and a length (l) of 0.076 m.
[b] The characteristic velocity (v) for a C-CORE experiment is 5×10^{-5} m/s with a gravity (g) of 160 and a length (l) of 0.904 m.
[c] The characteristic velocity (v) for the prototype is 1.5×10^{-10} m/s with a gravity (g) of 1 and a length (l) of 45×10^{3} m.

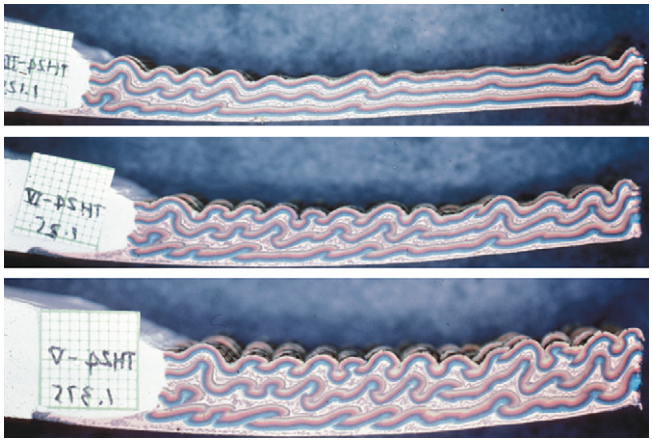

Fig. 3. Vertical sections of prototype model TH24 at stages III through V deformed in the Queen's centrifuge (Liu and Dixon, 1990). The labels are 1 cm^2 for scale (the photos are purposely mirrored to present the foreland end of the model at the right).

continued deformation, the buckle fold train propagated further toward the foreland in both upper and lower competent units. In addition, the hinterland region of the lower competent unit that was previously pervaded by buckle folds developed into a series of fold-thrust structures with regular spacing and consistent structural style. Newly developed buckle folds formed toward the foreland end of the model during the final stage of deformation (labeled as structures S_4 through S_7 in Figs. 5b and 6b).

In accordance with dynamic scaling theory, the C-CORE models and the models deformed at Queen's University show a similar structural evolution with the formation of geologically realistic fold-thrust structures from horizontal plane layers. The buckle folds and thrust structures nucleate from the hinterland to foreland as observed in natural fold and thrust belts as well as the earlier Queen's models. In addition, for this arrangement of competent and incompetent units there is a clear large-scale relationship between folding and thrusting: the buckle folds form first, and thrusts subsequently cut through the forelimb of the folds.

3.2. Strain partitioning in model fold-thrust systems

The lower competent unit of models TN16 and TN17 developed fold-thrust structures that accommodated the horizontal shortening and vertical thickening by three complementary mechanisms: buckle folding, imbrication on thrust faults, and distributed bulk strain layer-parallel shortening ("LPS"). Bed length measurements of the lower competent unit are used to determine the percentage shortening that is attributed to LPS and the reverse-sense shear bands. Bedding-offset is measured parallel to fault planes (for offsets greater than 3 mm) to determine the total shortening by fault slip, and shortening by folding was assumed to account for the remainder of the overall shortening. Mulugeta and Koyi (1987), Liu and Dixon (1990), Mulugeta and Koyi (1992) and Koyi (1995) employed this same technique to analyze strain partitioning during the development of model fold-thrust systems. The percentage of shortening accommodated by these three mechanisms is compared to the models deformed at Queen's University and a natural prototype system in Table 4.

Table 2
Stratigraphic unit thicknesses, number of laminae, and thicknesses of the silicone putty and plasticine laminae for models TN16, TN17 and model TH24, an equivalent model deformed in the Queen's centrifuge (Liu and Dixon, 1990).

Model	Unit	Silicone Putty to Plasticine Ratio	Unit Thickness (mm)	# Laminae	Plasticine Laminae Thickness (mm)	Silicone Putty Laminae Thickness (mm)
TN16	V	1:1	12	48	0.25	0.25
	IV	–	15	64	0.23	–
	III	1:1	6	48	0.13	0.13
	II	–	20	64	0.31	–
	I	1:1	6	48	0.13	0.13
TN17	V	1:1	12	48	0.25	0.25
	IV	–	16	64	0.25	–
	III	1:1	4	48	0.08	0.08
	II	–	19	64	0.30	–
	I	1:1	6.5	48	0.14	0.14
TH24	VI	–	1	4	0.25	–
	V	2:1	0.33	4	0.06	0.11
	IV	–	1	4	0.25	–
	III	2:1	0.33	4	0.06	0.11
	II	–	1	4	0.25	–
	I	2:1	0.33	4	0.06	0.11

The proportion of strain accommodated by each deformation mechanism is comparable for all three models and gives us confidence that the models are correctly scaled. All models show that a significant proportion of strain, over 50% of the total shortening, is accommodated by LPS and shear band development. A comparable proportion of strain accommodated by LPS is also observed in a natural duplex system; Kulander and Dean (1986) studied the Waynesboro thrust sheet to find that layer-parallel shortening reached almost 50% of the bulk shortening. Model TN17 has slightly more strain accommodated by displacement on thrust ramps than TN16, likely because its middle incompetent unit III is thinner (2 mm, or 100 m at prototype scale). This provides greater coupling of the competent beams, increases the structural wavelength and in turn inhibits fold shortening, producing longer-wavelength lower-amplitude folds. This result highlights that modeling results are sensitive to initial layer thicknesses of the competent and incompetent units.

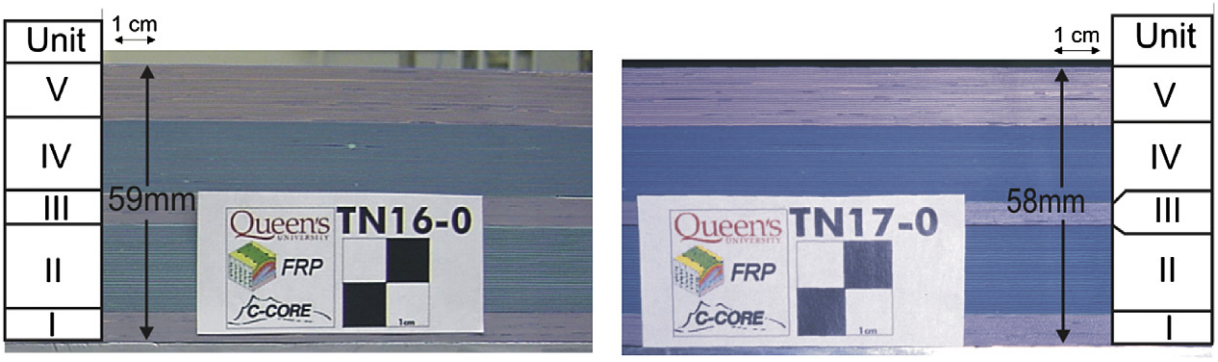

Fig. 4. Initial configurations of models TN16 and TN17, each composed of five internally layered stratigraphic units of alternating bulk competency, with an incompetent unit at the base (labeled as units I through V). Table 2 details the layer compositions and thicknesses.

Table 3
Summary of horizontal shortening for models TN16 and TN17.

Model	Initial Length (mm)	Shortening Rate (mm/s)	Stage I Bulk Shortening (%)	Stage II Bulk Shortening (%)	Total Bulk Shortening (%)
TN16	904	0.05	15	20	35
TN17	913	0.05	15	25	40

4. Temporal evolution of fold-thrust structures and timing of deformation mechanisms

The series of fold-thrust structures in the lower competent unit of model TN16 demonstrates the complete evolution of a geologically realistic overthrust structure initiated from horizontal plane layers. The large number of passive laminae allows a detailed structural interpretation of the individual structures, complete with folding and faulting relationships, the distribution of contraction faults, and the timing and intensity of internal strain accommodation mechanisms.

4.1. Documenting internal strain accommodation mechanisms

Thrust sheets develop deformation fabrics during emplacement. To the field geologist the deformation fabrics are essential for reconstructing and understanding the kinematics of fold-thrust development. Price (1967), Wojtal and Mitra (1986), and Wojtal (1986), among others, have documented the types of deformation fabrics related to thrust sheet emplacement in foreland fold-thrust belts at shallow crustal levels. Although the model materials in this study did not generate the exact same suite of mesoscopic subfabrics as rock systems during overthrust development (brittle faults, fractures, stylolites, *etc.*), it is instructive to compare the deformation mechanisms active in the analog centrifuge to those documented from natural overthrust structures.

The lower competent unit of models TN16 and TN17 developed arrays of small, planar, low-angle deformation bands that range in style from very subtle kinks to faults with discrete offset between beds. For simplicity, we herein refer to these features as contraction faults. The contraction faults accommodate horizontal shortening by vertical thickening of the units, and partition the competent units into a series of fault-bounded blocks (Figs. 5b, 6b and 7). We examined the pattern of these contraction faults in the lower competent unit of model TN16 in detail. The faults are easily identified and mapped as continuous offsets of the bedding laminae in the competent unit. The contraction faults were initially planar and appear to have formed at consistent angles relative to bedding, between 30° and 35° to the structural dip of the bedding laminations. For these initially planar contraction faults, the intersection angles between bedding and contraction fault remained constant along the length of the fault plane from the upper and lower boundaries toward the center of the unit. After the generation of contraction faults, thrust sheets accommodate additional internal horizontal shortening and vertical thickening by homogeneous LPS, and by the displacement and rotation of blocks that are bounded by contraction faults. These internal deformation mechanisms can be distinguished by variations in the bedding-fault intersection angles ("∠B–F"), the angles between the bedding laminations and the planar contraction faults. Three end-member situations exist: if no additional internal strain is accrued then the ∠B–F remain the constant at 30–35°; if internal strain is accommodated by homogeneous LPS then the ∠B–F increase; and lastly, additional strain that is accommodated by rotation of fault-bounded blocks decreases the ∠B–F (Fig. 7). Measuring and contouring ∠B–F along all the contraction faults allows the identification of locations on an overthrust structure where subsequent strain is accommodated by either LPS or rotation of fault-bounded blocks.

4.2. Temporal evolution of fold-thrust structures

The temporal evolution of a fold-thrust structure in initially planar continuous layers can be constructed from the observation of structures ranging from tectonically immature structures in the foreland toward more mature structures in the hinterland, and taking these as a pseudo-temporal representation of the evolution of a single structure. This evolution is illustrated in the lower competent unit of model TN16. Fig. 8 shows the pseudo-evolution of such a structure by first presenting structure S_7, in the immature stages of development, then sequentially presenting progressively more mature structures through to structure S_2. The contraction faults were mapped on the photographs and the ∠B–F were measured along each fault. Measurements of ∠B–F throughout the overthrust structures of differing maturity were contoured to display the relative timing, location and intensity of internal strain accommodation mechanisms.

S_7 (immature) (Fig. 8a and b): A very low-amplitude fold represents the incipient strain as the first-order buckling instability steps out toward the foreland (Fig. 8a). Regularly spaced and consistently oriented foreland-verging contraction faults span the fold and horizontally shorten and vertically thicken the unit. Contraction faults that originate at the base of the unit are initially planar and form consistent angles of 30–35° to the structural dip of the bedding laminations. The displacement on the contraction faults is greatest at the boundaries of the competent units, diminishing to zero at various distances inwards from the boundaries.

In conjunction with development of early contraction faults, LPS accommodated shortening during early stages of overthrust development. ∠B–F increases moderately along contraction faults toward the center of the unit in tectonically immature structures from ~30° at the boundary to a maximum of ~40° toward the center of the unit where displacement dies out (Fig. 8b). Shortening appears to be accommodated by displacement on faults near the boundary of the unit and additionally by LPS in the center of the unit where displacement on contraction faults diminishes, increasing ∠B–F.

S_6 (Fig. 8c and d): With continued shortening, the buckle fold grows in amplitude and develops a pronounced foreland vergence. At this stage the fold is most similar to a detachment fold, where the fault slip is horizontal and distributed within the underlying incompetent unit. A set of hinterland-verging contraction faults develops across the asymmetric first-order buckle folds, originating at the upper boundary of the competent unit. The sense of displacement of the faults that originate at the upper boundary is opposite to that of the contraction faults that originate from the bottom of the layer, suggesting that a form of tectonic wedging is taking place as the fold-thrust structure is horizontally shortened and vertically thickened by displacement on conjugate shear surfaces. Contraction faults that develop at the upper boundary of the competent unit proximal to the crest of the fold are subsequently folded during development of the asymmetric buckle-fold.

S_5 (Fig. 8e and f): As the structure develops into a distinct detachment fold, the concentration of foreland-verging contraction faults increases modestly in the back limb but increases dramatically in the forelimb. From the orientations of the contraction faults one can infer that the axis of maximum stress is plunging toward the foreland more steeply in the forelimb of the fold than in its back limb. Planar contraction faults that are partially incorporated into the hanging-wall syncline develop a curvilinear shape as the back limb is back-rotated during fold development.

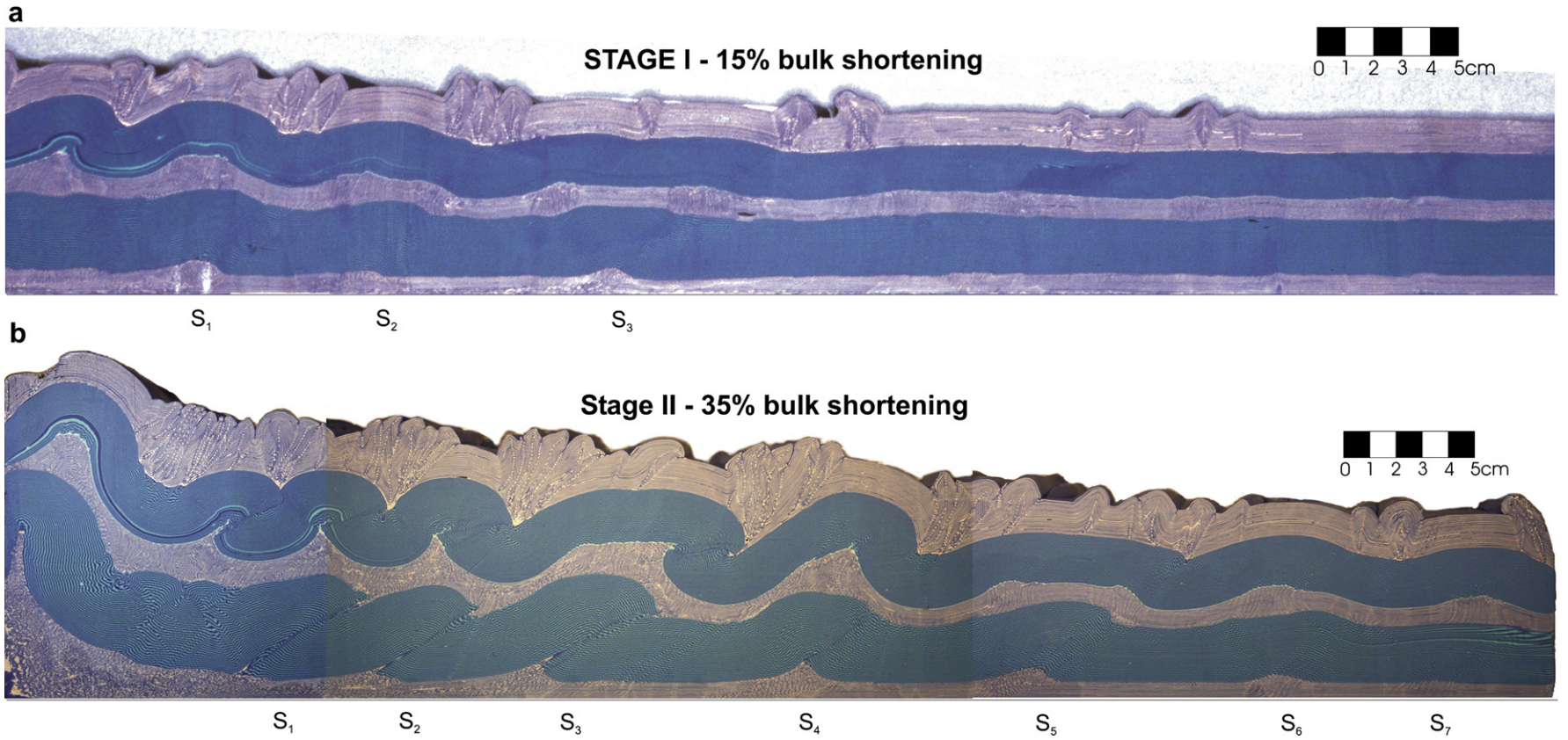

Fig. 5. Transverse profiles of model TN16 taken after (a) Stage I, and (b) Stage II of deformation. The buckle folds and associated thrust structures that subsequently develop are labeled in order of their sequential development on both the stage-I and stage-II photographs.

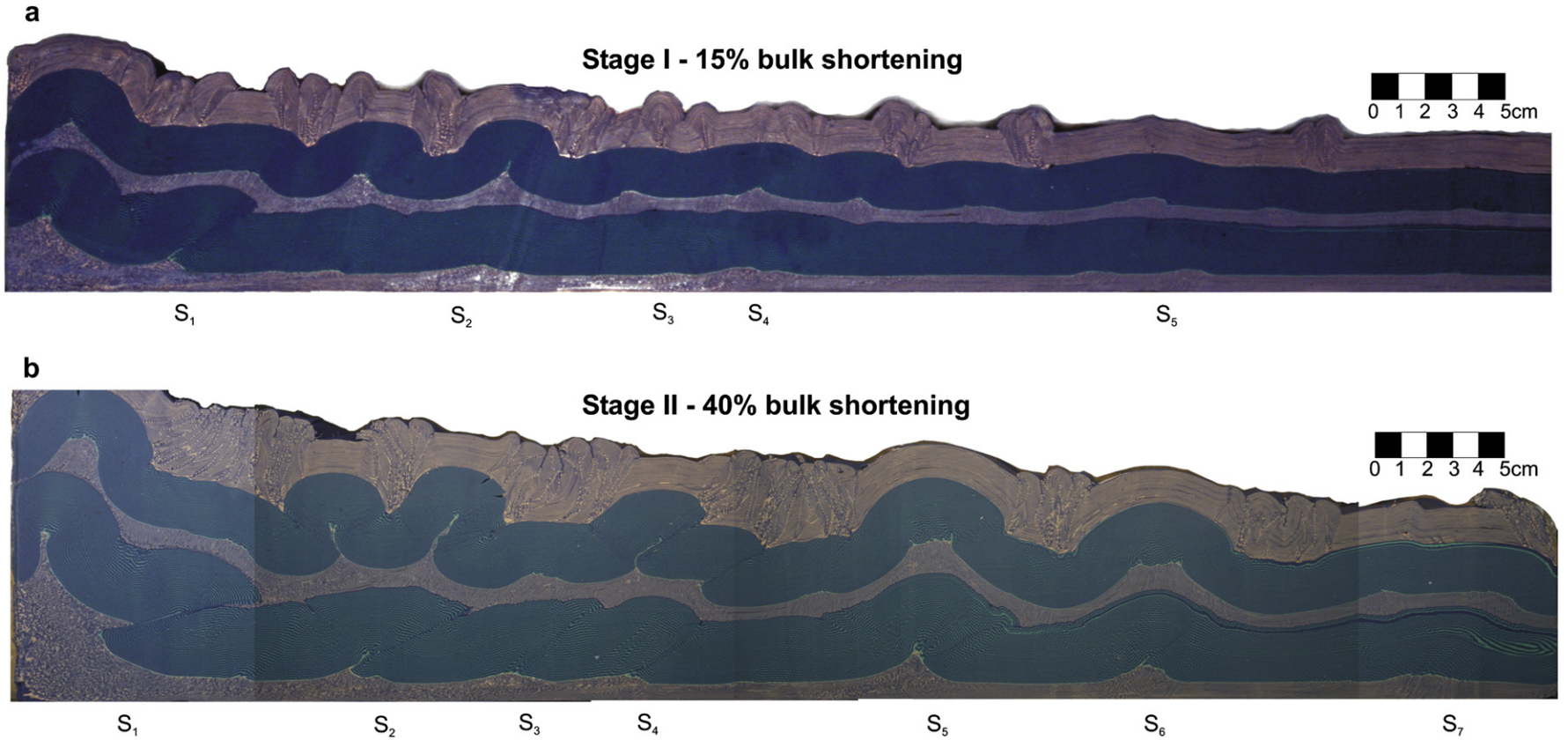

Fig. 6. Transverse profiles of model TN17 taken after (a) Stage I, and (b) Stage II of deformation. The buckle folds and associated thrust structures that subsequently develop are labeled in order of their sequential development on both the stage I and stage II photographs. A section of undeformed strata is omitted from the foreland end in the stage-I photo.

Table 4
Summary of the shortening and strain partitioning in models TN16, TN17 and TH24, as well as a prototype with comparable structural style, the Waynesboro thrust sheet in of the Appalachian Valley and Ridge Province (Kulander and Dean, 1986). The values in brackets represent the percentage of the total shortening accommodated by each mode of deformation.

	Fold shortening (fraction of total shortening)	Thrust shortening (% of total shortening)	LPS shortening (fraction of total shortening)	Total shortening
TN16	9% (25%)	6% (17%)	20% (57%)	35%
TN17	6% (17%)	8% (20%)	24% (63%)	38%
TH24	13% (23%)	12% (20%)	33% (58%)	58%
Waynesboro Thrust Sheet, Appalachian Valley and Ridge Province	Range of 24–32% (combined)		Up to 30% (Up to 60%)	~50%

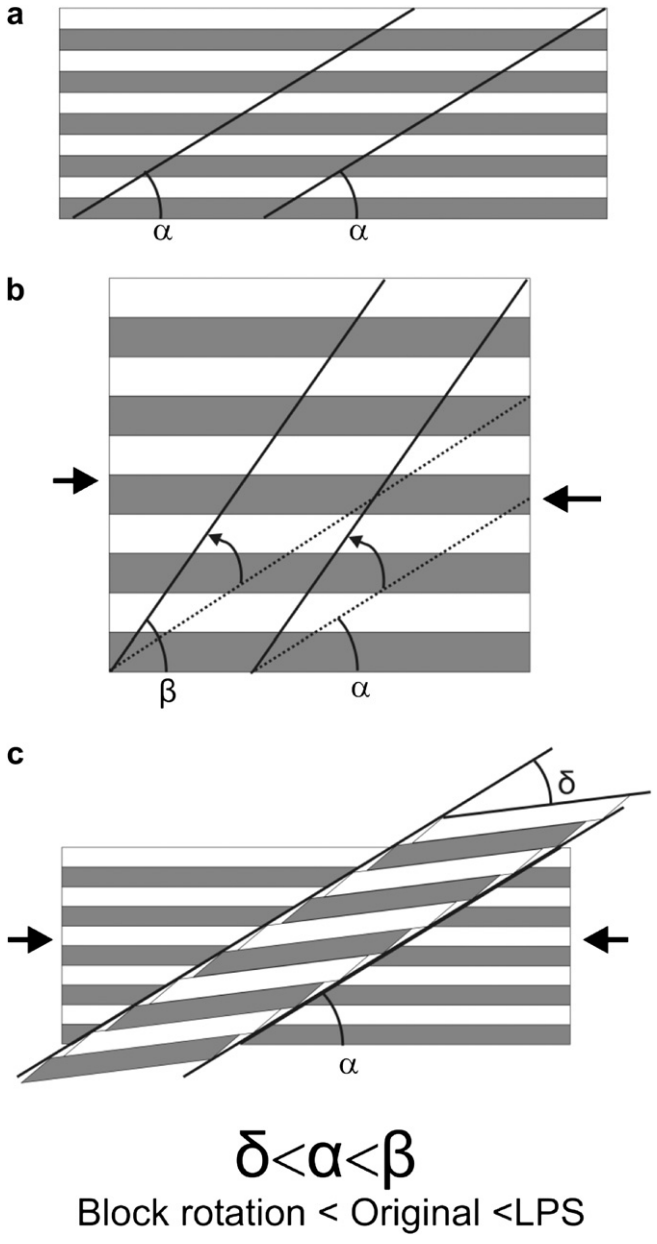

Fig. 7. Influence of internal strain accommodation mechanisms on bedding-fault intersections ("∠B–F"). (a) Undeformed bedding laminations with contraction faults that maintain a constant ∠B–F, such that $\alpha = \alpha$. (b) Homogenous LPS of the sequence increases the ∠B–F, and $\beta > \alpha$. (c) Back-rotation of a fault-bounded block accommodates horizontal shortening by vertical thickening, decreasing ∠B–F, and $\delta < \alpha$.

Some curviplanar faults that form in the syncline beneath the fold's forelimb also fit the model of out-of-syncline fold-accommodation faults described by Mitra (2002). Out-of-syncline faults develop to accommodate additional strain where bed-curvature is increased in the core of the syncline. Consistent with Mitra's (2002) model, these faults are curviplanar and steeply hinterland- dipping, but only appear to develop on the steeply dipping limp of the synclinal fold.

S_4 (Fig. 8g and h): In thrust structure S_4, a fault propagates halfway through the forelimb of the buckle fold, and displacement on the thrust ramp diminishes to zero at the fault tip. Folding of the hanging-wall panel accommodates strain ahead of the propagating thrust tip. At the leading edge of the hanging-wall panel, folding and steepening of the forelimb are facilitated by relative displacement and forward-rotation of fault-bounded blocks, and are indicated by decreased ∠B–F. Fault-bounded blocks in the core of the fold, in the region of the greatest bulk strain, are back-rotated, decreasing ∠B–F. The fault-bounded blocks in the hanging-wall syncline of structure S_4 are back-rotated as the cumulative amount of internal strain in the hanging-wall panel increases during development of this fault-propagation fold.

S_3 (Fig. 8i and j): With continued propagation of the fault and associated folding of the hanging-wall panel, the fault tip cuts through the entire forelimb of the fold on a synclinal breakthrough trajectory. Small thrust horses are cut from the hanging-wall and footwall panels adjacent to thrust, indicating that several fault planes are active during overthrust development. At this stage, the concentration of consistently oriented contraction faults at the base of the hanging-wall panel increases dramatically as the thrust sheet accommodates internal shortening during displacement. When the fold shape reaches maturity and the main thrust begins to cut through the forelimb, the hanging-wall panel accommodates a greater amount of internal strain during displacement of the thrust sheet. At the leading edge of the hanging-wall panel, continued folding and thinning of the forelimb is facilitated by relative displacement and forward-rotation of fault-bounded blocks as bedding is overturned ahead of the propagating thrust ramp. After the fault cuts through the entire forelimb the hanging-wall panel is transported along the footwall ramp to become the transported fault-propagation fold (Fig. 8i).

5. Geometric analysis of individual fold-thrust structures and kinematic implications

The fold-thrust structures that develop in the lower competent unit of model TN16 share many similarities to natural structures and appear geologically realistic. To demonstrate that this modeling technique is accurately simulating the tectonic evolution of fold-thrust structures, the geometry and kinematic evolution of model overthrust structures is compared with accepted geometric models and quantitative fold-thrust relationships derived from natural fold-thrust structures.

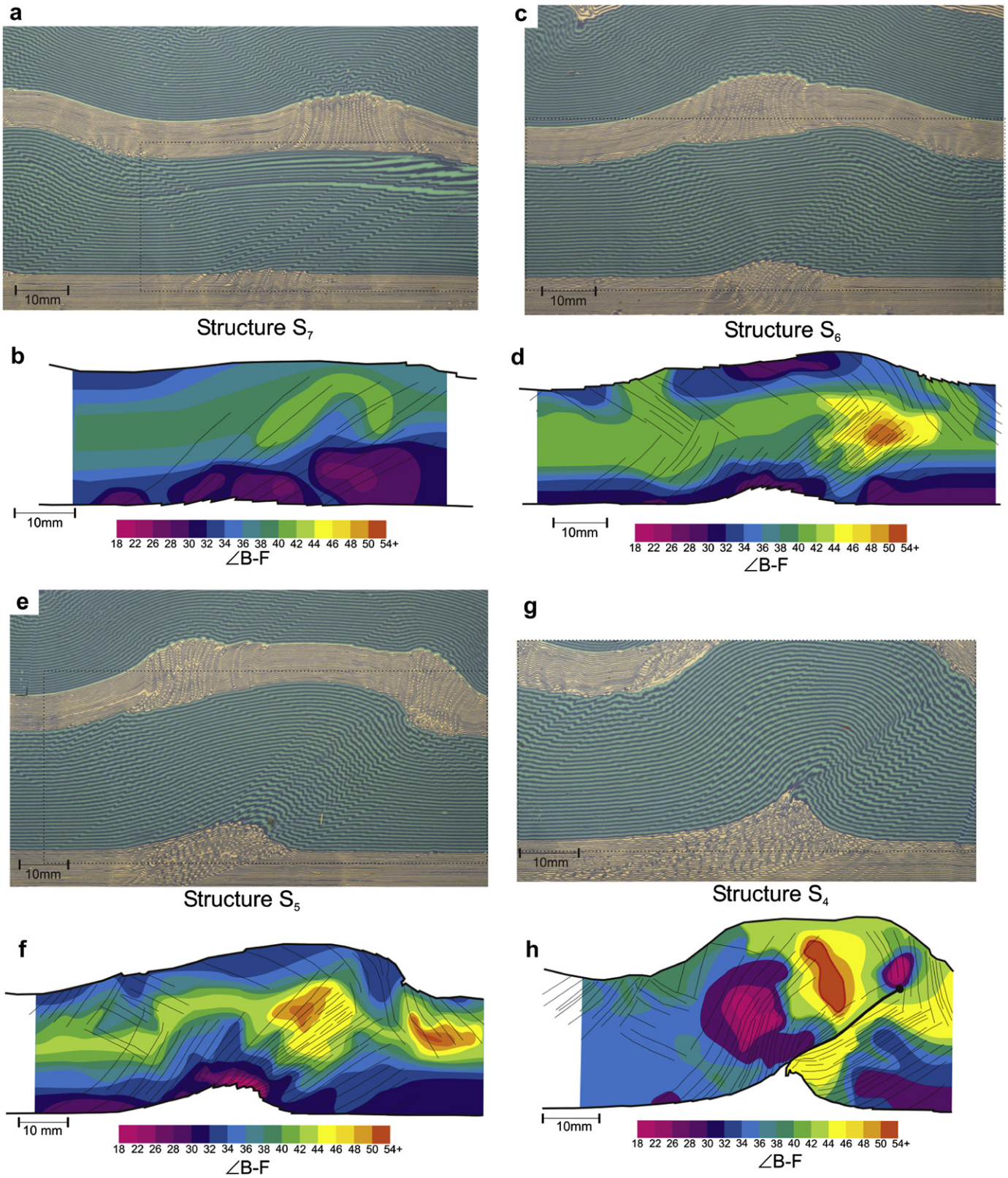

Fig. 8. Enlarged images of overthrust structures S_7, S_6 S_5, S_4, and S_3 in the lowermost competent unit of model TN16 (Fig. 5). Beneath each photo is the associated colored structural interpretation showing the orientation and distribution of contraction fault arrays with contoured Bedding-Fault intersection angles ($\angle$B–F) shown in the background. The portion of the image that is interpreted is outlined by a dashed box.

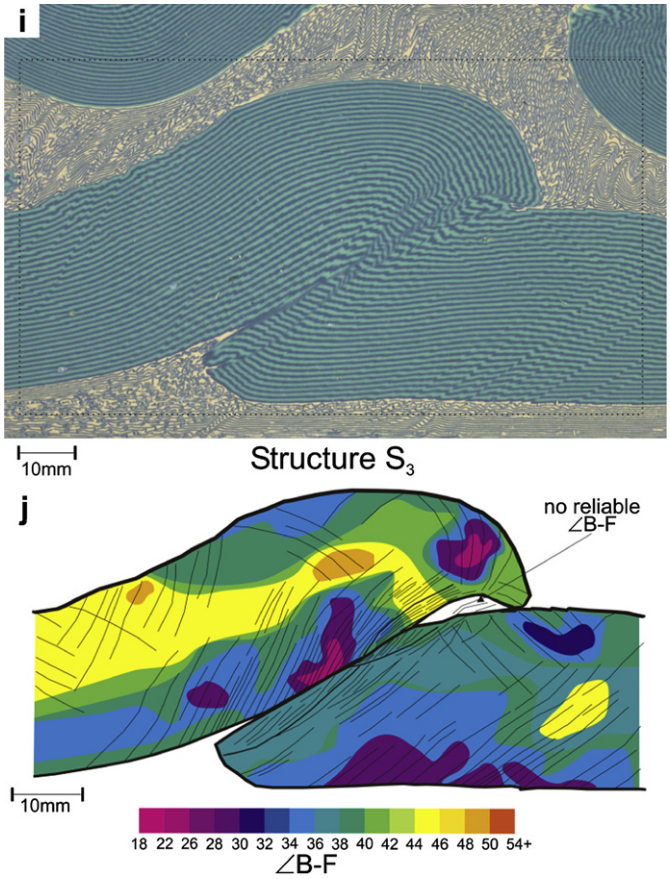

Fig. 8. (Continued)

5.1. Relative stretch in model fold-thrust structures

During the development of fault-propagation folds, tectonic shortening is simultaneously accommodated by displacement of the hanging-wall panel along the thrust ramp and by folding of the hanging-wall panel. Folding of the hanging-wall panel steepens the forelimb and shortens the length of the hanging-wall panel adjacent to the thrust ramp. The resulting length mismatch between the hanging-wall and footwall panels is called the relative stretch (ε_r) and is expressed by a percentage of thinning or thickening (Eby et al., 1923; Dahlstrom, 1970; Williams and Chapman, 1983). The relative stretch can be easily determined for fault-propagation folds by calculating the ratio of the measured lengths of the hanging-wall and footwall cutoffs parallel to the thrust. As is observed in natural prototype structures, overthrust structures in model TN16 have hanging-wall cutoffs that do not match footwall cutoffs because of differences in the internal strain above and below the thrust. The relative stretch values measured on model TN16 structures for S_2, S_3, S_4 and S_5 are 0.84, 0.80, 0.75 and 0.90 respectively (Fig. 9). This shows that all of the hanging-wall panels have undergone progressive folding during the propagation of the underlying thrust fault. A smaller relative stretch (ε_r) value indicates a greater amount of fold shortening accrued during structural development.

5.2. Comparison with geometric models for fault-propagation folding

Suppe (1983) and Suppe and Medwedeff (1990) derived a suite of curves relating the fold inter-limb angles to the ramp angle for fault-bend and fault-propagation folds. They applied a number simplifying assumptions to their solutions: bed length is conserved, folds have straight limbs, folds evolve self-similarly by parallel kink-band folding, and deformation occurs by layer-parallel slip. Jamison (1987) expanded on this work by producing a similar set of curves that incorporate thickening or thinning of the forelimb for fault-propagation, fault-bend and detachment folding. Jamison's (1987) charts were intended to predict the mode of structural deformation from inter-limb and ramp angles, while also correctly estimating the thinning or thickening of the forelimb. The inter-limb angles versus ramp angles of model TN16 structures S_2, S_3, S_4 and S_5 are plotted on Jamison's (1987) charts for comparison to theoretical geometries (Fig. 10). Since the analog models in this study do not deform through the exact mechanisms and assumptions used for the geometric models, we can expect differences

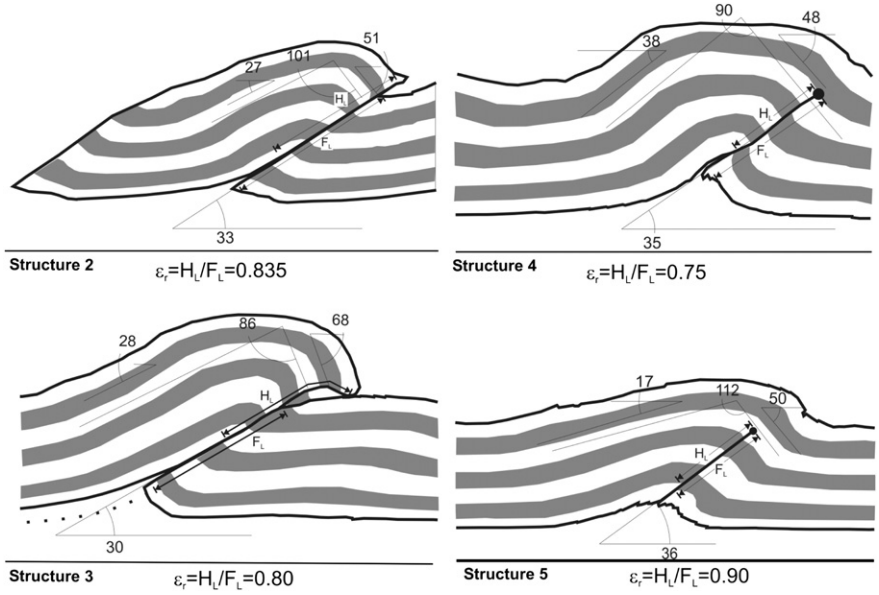

Fig. 9. Structural outlines of fold-thrust structures in the lowermost competent unit of model TN16. The fold inter-limb angles and ramp angles are labeled on each structure. Relative Stretch values are calculated using the length of the hanging-wall and footwall ramps parallel to the thrust.

between the model structures and the theoretical geometries. In general, the model fold geometries plot within the possible range of geometries predicted by theoretical kink-band style models.

In structures S_4 and S_5 the fault has cut partially through the forelimb of the fold. The corresponding points for these structures are plotted on the fold geometry chart for fault-propagation folds (Fig. 10a). The forelimbs of structures S_4 and S_5 have been thickened by fault imbrication and LPS during development of the asymmetrical detachment fold. The absolute quantity of forelimb thickening predicted by the geometric model for structure S_5 does not match closely but the geometric model correctly identifies that the structure would have thickening in the forelimb. The geometry for structure S_5 plots on the border of the 'no solution' space for the geometric model, which suggests its geometry is not compatible. Plotting the fold geometry for structure S_4 also does not correctly predict the thinning of the forelimb in the hanging-wall panel ($S_4 = 0\%$). Although the forelimb of structure S_4 had initially been thickened during fold development, it subsequently experienced 25% thinning of the hanging-wall panel relative to the footwall during fault-propagation folding.

Structures S_2 and S_3 have thrust faults that cut entirely through the forelimb of the fold and the thrust sheets are transported along the ramp, thus are plotted on the chart for transported fault-propagation folds (Fig. 10). The forelimbs of the hanging-wall panels have been thinned due to folding ($S_2 = 14\%$, $S_3 = 22\%$), and these compare favorably with the predicted percentage of forelimb thinning for both fold geometries ($S_2 = 20\%$, $S_3 = 20\%$).

5.3. Geometric relationships in fault-propagation folding

The relative stretch (ε_r) is a function of the amount of shortening that is accommodated by folding in the hanging-wall panel and the amount accommodated by fault slip. Relative stretch can also be expressed as a ratio of fault slip to fault-propagation (S/P) during development of the overthrust structure (Williams and Chapman, 1983). The manner in which displacement diminishes along a thrust fault in a fault-propagation fold is an indicator of the relative stretch and fault slip to propagation ratio, *i.e.,* constant displacement along the fault would indicate no relative stretch and infinitely small S/P ratios (i.e. fault-bend fold), whereas rapidly diminishing displacement indicates high relative stretch and larger S/P ratios (*i.e.,* fault-propagation folding). On a plot of fault displacement vs. distance along the fault for fault-propagation folds, the slope represents the relative stretch, ε_r, and changes in the slope represent variations in thrust propagation rates (Williams and Chapman, 1983).

Transverse sections of model TN16 cut parallel to the direction of fault slip provide full exposure of all the fault-propagation folds in the lower competent beam and allow the displacement to be measured along the entire length of the thrust faults that propagate through the forelimbs of the folds. For example, the displacement-distance diagram for structure S_4 of model TN16 is shown in Fig. 11a. A theoretical relationship exists between the gradient measured from a displacement-distance diagram and the predicted relative stretch value (Fig. 11b). Gradient values for structures S_2, S_3 and S_4 plotted on the theoretical curve yield relative for stretch values of 0.81, 0.75 and 0.77 respectively. These are consistent with the relative stretches calculated as a ratio of hanging-wall and footwall lengths measured parallel to the thrust ($S_2 = 0.84$, $S_3 = 0.80$, $S_4 = 0.75$).

6. Discussion

The fold-thrust structures that developed in model TN16 appear to simulate closely the geometry and kinematic development of natural structures. The model fold-thrust structures demonstrate consistency with conceptual models such as the break-thrust model proposed by Willis (1893) and the smooth-trajectory thrust illustrated by Cooper and Trayner (1986). The fold geometries, including ramp angles and forelimb thickening and thinning, fit within the bounds of geometric models for detachment and fault-propagation folds (Jamison, 1987), as well as capturing the simultaneous interaction of folding and thrusting that is characteristic of fault-propagation folding (Suppe and Medwedeff, 1990). In these models the development of foreland-verging folds yields forelimb thickening of approximately 20% (e.g. structure S_5). Fault-propagation folding subsequently overprints this forelimb thickening by thinning the hanging-wall panel by ~20% with passage of a major thrust fault (e.g. structures S_3 and S_4). This overprinting leads to an erroneous estimate of forelimb thinning from ramp and inter-limb angles, i.e. $S_4 = 0\%$, and indicates that for accurate application of geometric models one must deconvolve the penetrative strain associated with folding and thrusting events. Koyi and Teixell (1999) advised similar caution when applying geometrical models for section-balancing in thrust systems that result from a combination of brittle deformation at shallow levels and ductile deformation deeper in the section.

Passive laminae behave as strain markers that capture high-resolution snap-shots of the deformation throughout a structure's evolution. The density and distribution of contraction faults can be easily mapped on these structures. The greatest intensity of

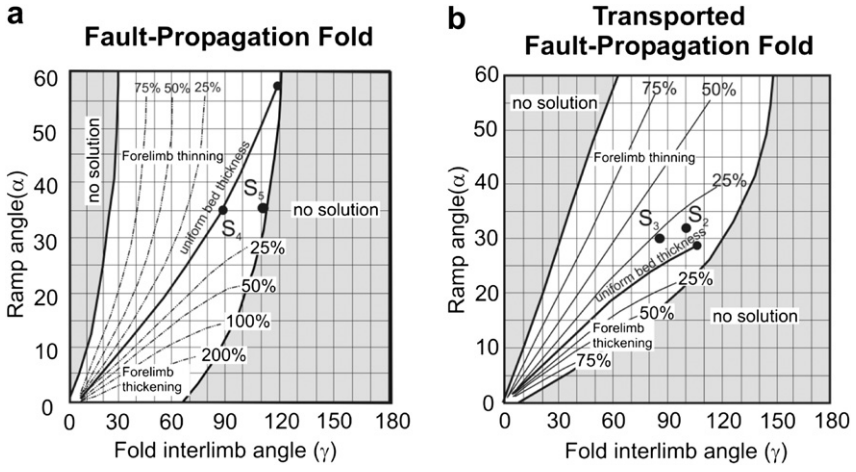

Fig. 10. Model TN16 fold geometries ($S_{2,3,4,5}$) plotted on graphical representations for the geometric analysis of (a) developing and (b) transported fault-propagation folds. Curves relate fold inter-limb angle (γ) to ramp angle (α) for specified amounts of forelimb thinning and thickening for geometric models of fault-propagation folds. (After Jamison, 1987).

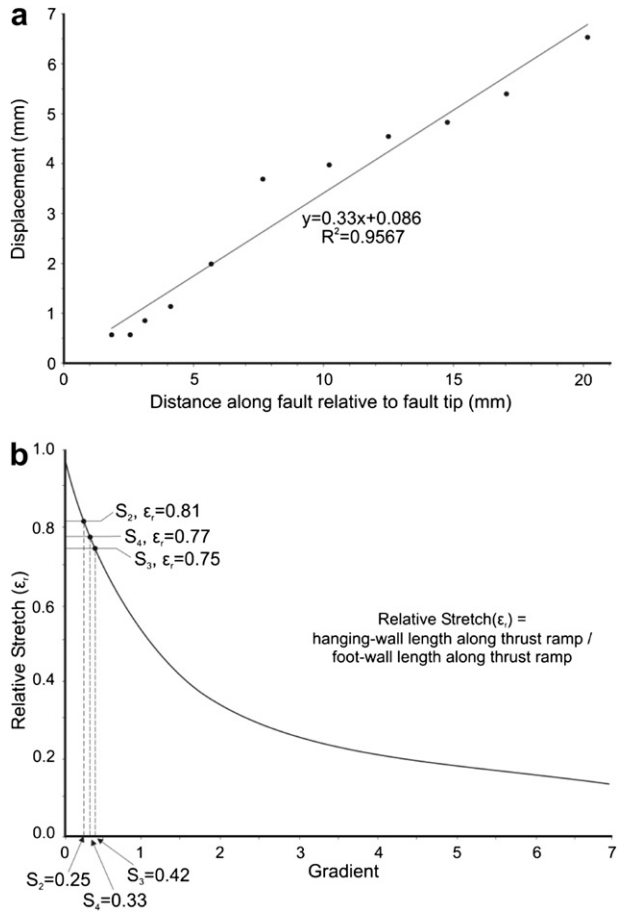

Fig. 11. (a) The displacement-distance diagram for structure S_4. (b) A graph showing the relationship between the gradient on the distance-displacement diagram and the relative stretch (ε_r) between the hanging-wall and footwall panels for structures $S_{2,3,4}$ (After Williams and Chapman, 1983).

contraction faults occurs in the forelimbs of folds and proximal to main thrust faults as foreland-verging faults that nucleate at the lower boundary of the competent unit. Similar distributions of faults have been noted in natural structures; thrust sheets in the Appalachians also exhibit a similar deformation style where families of consistently oriented minor fault populations accommodate horizontal shortening and vertical thickening of rocks nearest to the thrust (Wojtal, 1986). Model structures also develop a conjugate set of hinterland-verging contraction faults; the majority form early in the tectonic shortening and appear indicative of tectonic wedging (structures S_5 and S_6); some are subsequently warped by fold-limb rotation and fold development; and a relatively small number form later on as out-of-syncline faults (e.g. structure S_4 in Fig. 8g) (Mitra, 2002).

The angular relationship between bedding and contraction faults reveals regions where LPS and rotation of fault-bounded blocks are active in the structural evolution. In the early stages of folding LPS is dominant in the center of the competent beam and the forelimb of the fold. Observation of the progressive evolution of structures in the lower competent unit of model TN16 demonstrates that strain is quickly focused in the forelimb of growing folds. For example, at incipient stages of folding the reverse-sense shear bands are distributed evenly across the structures but the fault-bounded blocks are measurably thickened in the forelimb by LPS (e.g. Structure S_7). At early stages of folding, e.g. S_6 with inter-limb angles $\sim 140^\circ$, the strain is clearly concentrated in the forelimb in the form of contraction faults, LPS and rotation of fault-bounded blocks even though the fold only has slight foreland vergence. In structures at mature stages of folding, e.g. S_4 & S_3, the forelimb of the structure undergoes the greatest total bulk strain and the hanging-wall panel remains relatively undeformed. Bedding-fault angles in fault-propagation folds and transported fault-propagation structures (structures S_4 and S_3 shown in Fig. 8g and i) do not reveal pronounced LPS in the forelimb, likely because it is subsequently obscured by intense faulting proximal to the main thrust fault.

The rotation of fault-bounded blocks throughout the evolution of model fold-thrust structures shows how pre-existing fabrics play a role in the subsequent accommodation of internal strain in the hanging-wall panel. When the main thrust faults cut through the forelimb of the hanging-wall panels in structures S_4 and S_3, continued folding and thinning of the forelimbs is facilitated by relative displacement and forward-rotation of fault-bounded blocks as bedding is overturned ahead of the propagating thrust ramp. Wojtal (1986) likened the ductile deformation accrued by displacement and rotation of blocks bounded by contraction faults that occurs during emplacement of a thrust sheet to mesoscopic grain-boundary sliding, and provided examples from the Copper Creek, Hunter Valley and Cumberland Plateau thrusts in the southern Appalachian Valley. Displacement-distance relationships along fault planes in natural structures reveal variability in the nucleation points for faults in a stratigraphic sequence and variations in the distribution of fault slip (Ellis and Dunlap, 1988; McConnell et al., 1997; Nicol et al., 1996). The displacement-distance data for structure S_4 in model TN16 reveal that the fault nucleates at the lower boundary of the competent unit and displacement decreases toward the fault tip. A slope change of the trend on the displacement-distance diagram for structure S_4 shows that the fault tip propagated rapidly through the lower section of the forelimb and then slowed through the upper section of the forelimb (Fig. 11a). The relatively high concentration of contraction faults in the lower part of the forelimb likely facilitated displacement on a main thrust ramp then slowed as the fault tip cut through the upper, less-deformed portion of the forelimb. Chapman and Williams (1984), stated that a non-linear, or inflected, slope on a displacement-distance diagram can result from changes in lithology through which the fault propagates. We would like to extend this statement to include the possibility that a slope change in a displacement-distance diagram may be indicative of the fault cutting through a zone of pre-existing strain that weakened the rock, implying that major thrusts cut faster through weakened zones. To further support this point, structure S_5 captures development of a major thrust zone through the lower, deformed portion of the forelimb and the displacement-distance diagram states a stretch of 0.90, or relatively fast propagation.

The values of relative stretch determined from the model structures in model TN16 are in close agreement with those commonly observed in natural fold-thrust structures. Natural fold-thrust structures described by Chapman and Williams (1984) with a relative stretch of ~ 0.75 share a similar evolutionary history and geometry to those in model TN16. The asymmetrical fold grows well in advance of the propagating thrust, creating steeply dipping beds in the forelimb and a footwall syncline; a thrust then cuts up-section through the forelimb of the fold with a fault slip to fault-propagation ratio that is less than 1, that further modifies the fold profile by overturning the beds in the hanging-wall immediately in front of the thrust (Chapman and Williams, 1984). The relative stretch can be expressed as a ratio of fault-propagation to fault slip, $\varepsilon_r = 1 - (\mathrm{Fault}_{\mathrm{slip}}/\mathrm{Fault}_{\mathrm{propagation}})$. Given that the relative stretch values observed in the model TN16 structures are geologically reasonable, the ratio of fault slip and fault-propagation should also be comparable to those observed in natural fault-propagation folds.

Close examination of structure S_3 (Fig. 8i) shows that undeformed, flat laminae in the lowermost incompetent unit (unit I) are

transported over a thrust ramp that has a listric trajectory, flattening down-dip toward the hinterland within the lowermost incompetent unit. The down-section continuation of the thrust ramp cuts through highly deformed and overturned buckle folds in the silicone putty and plasticine lamine. Examination of the temporal development of the thrust structures leads to the conclusion that the thrust ramp initiated at the lower boundary of the competent unit and propagated up-section through the forelimb of the buckle fold, rather than propagating upward from within the underlying incompetent unit. It appears that as the thrust ramp cut up-section through the forelimb of the competent unit toward the foreland, it simultaneously cut down-section toward the hinterland into the underlying incompetent unit and through the region of overturned higher-order buckle folds. Eisenstadt and De Paor (1987) proposed a similar theory whereby a fault nucleates as a ramp cutting a competent unit, and propagates both up-section and down-section until it reaches an incompetent layer and turns parallel to bedding.

Brittle deformation is known to enhance the deliverability of some oil and gas reservoirs in prototype fold-thrust structures. These models show that for a thick, uniform beam of competent rock the forelimb of the fold-thrust structure has the highest intensity of reverse-sense shear bands, major thrust planes and rotated of fault-bounded block. The intense brittle deformation in the forelimb of the fold-thrust structures is a consequence of forelimb thickening during fold development and subsequent forelimb thinning during fault-propagation folding, e.g. structures S_5, S_4 and S_3. The back limb regions of the model fold-thrust structures have a relatively lower degree of brittle deformation consisting of reverse-sense contraction faults and fault-block rotation. The crest portion of the model structures, especially upper half of the competent unit, is carried passively and remains relatively undeformed through fold growth. If an analogous situation applies in natural prototype structures and brittle deformation is necessary to increase reservoir performance then the forelimb region of the fold-thrust structures presents the most desirable target, having undergone multi-stage deformation with potentially cross-cutting deformation features. The back limb position may still be prospective if a relatively lower degree of brittle deformation is sufficient to improve reservoir performance. Lastly, the crestal position of the structure has minimal brittle deformation in the upper section of the competent beam and hence this region may not be a suitable target, unless underlying younger thrusts further enhance deformation.

7. Conclusions

Dynamically scaled physical analog modeling in a large geotechnical centrifuge presents an excellent opportunity to simulate the development of fold-thrust structures with full control over platen displacement rates. The large initial model size allows for complex initial stratigraphic and structural configurations. Stratigraphic units prepared with a “reversible sheeter” have fine bedding laminations as thin as 0.1 mm that act as strain markers and reveal a very detailed strain picture throughout deformation. The load-measuring devices mounted on the loading platen introduce the possibility of monitoring loads at the hinterland end of the model and detecting changes in the strength of a stratigraphic sequence as the models are shortened. This opens a future opportunity to investigate stress–strain relationships related to the timing and development of fold and thrust structures during a dynamically scaled experiment.

The individual models shown here illustrate and quantify fold-thrust features that can be scaled to naturally occurring structures. These include:

- Horizontally shortened plane-layered C-CORE models develop a series of regularly spaced, geologically realistic fold-thrust structures that nucleate from hinterland to foreland in the lower competent unit. An evolutionary relationship exists in the development of the fold-thrust system; the regular spacing of thrust ramps in the duplex structures is inherited from the buckling instability of the competent beam. At the scale of the fold-thrust system, strain is accommodated by homogeneous LPS, families of contraction faults, folding, and displacement on thrust faults.
- Fold-thrust structures in model TN16 document a complete structural evolution from initial plane layers to a transported fault-propagation fold. Model fault-propagation folds exhibit folding and thrusting relationships, including forelimb thinning and thickening, that fit accepted geometric models. Analysis of model structures demonstrates that to correctly apply these geometric models the strain episodes of forelimb thickening during folding and subsequent thinning during fault-propagation must be deconvolved.
- Displacement-distance data obtained from major thrusts in the model show relative stretch values, and consequently fault slip/propagation ratios, that are similar to natural structures. Inflected slopes on displacement-distance diagrams show that fault-propagation rates change throughout a fold-thrust structure’s development. It is interpreted that the strain fabrics associated with fold development impact the mechanics of fault processes, e.g. pre-existing brittle deformation fabrics weaken the rock and facilitate propagation.
- Variations in bedding-fault intersection angles $\angle$B–F indicate where the different deformation mechanisms are active within a fold-thrust structure and at what evolutionary stage they occur. Low-angle contraction faulting and LPS are prominent at the initial stages of buckle folding. Rotation of fault-bounded blocks occurs in forelimbs and back-limbs during progressive folding of the hanging-wall panel during fault-propagation folding. The progressive evolution of the model structures in model TN16 shows that strain is focused in the forelimb of a fold-thrust structure at very early stages of fold growth.
- Understanding the distribution and intensity of brittle deformation in fold-thrust structures through analog modeling is advantageous to the petroleum industry when production from hydrocarbon-bearing reservoirs is enhanced by fracturing and faulting. This analog modeling technique can help explorationists understand and potentially predict the strain intensity and distribution on natural fold-thrust structures. This provides impetus for continued experimentation using large centrifuges such as that at the C-CORE to better understand the structural evolution of natural fold-thrust structures.

Acknowledgments

The work reported here constitutes part of the M.Sc. research of T. Noble under the supervision of J.M. Dixon. TN gratefully acknowledges financial support in the form of a Natural Sciences and Engineering Research Council of Canada (NSERC) PGS scholarship, a McLaughlin Fellowship and CSEG scholarships. JMD acknowledges financial support of his research program from the industry sponsors of the Fold-Fault Research Project and NSERC. We thank Susan Pfister, Gerry Piercy and the technicians of the C-CORE centrifuge facility for their design of the testing rig and collaboration during testing sessions. TN would like to thank a colleague for his thoughtful reviews and suggestions that have improved this manuscript.

Appendix A

The rheological behavior of the two model materials, plasticine and silicone putty, and selected prototype rocks are represented in Fig. A1 for an experiment in the large geotechnical centrifuge at C-CORE. Data for the model materials are plotted against the lower and left-hand axes, and data for the prototype rocks are plotted against the upper and right-hand axes. To achieve dynamic scaling, with properly chosen stress and time ratios, the regions populated by the rheological data for the model materials should coincide with the rheological data for the corresponding prototype rocks. Since the model/prototype stress ratio (σ_r) is related to the model/prototype acceleration ratio (a_r), by the relationship

$$\sigma_r = \rho_r \times l_r \times a_r$$

where ρ_r is the model ratio of density and l_r is the model ratio of length, selecting a stress ratio that aligns the model and prototype stress/strain-rate curves constrains the appropriate acceleration ratio (**g**-level) for a particular set of centrifuge experiments with given model ratios of length (l_r), density (ρ_r) and time (*i.e.,* strain-rate). For this study, with its selected model ratios of strain-rate, length and density (shown in Table 1), to achieve this overlap the strain-rate axes in Fig. A1 are offset horizontally by a time ratio of 10^{-11} (1 h in the model = 11.5 Ma in the prototype), and the stress axes are offset vertically by a stress ratio of 0.0019 (model/prototype). This corresponds to models deformed at 3200 **g** in the Queen's centrifuge, and models deformed at 160 **g** at the C-CORE Centrifuge. See also Dixon and Summers (1985).

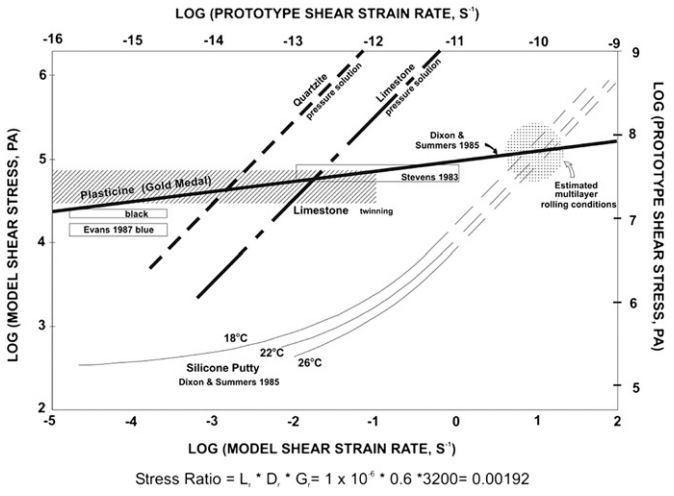

Fig. A1. Shear stress vs. shear strain-rate plot illustrating the rheological behavior of model materials (silicone putty and plasticine) and some natural prototype rocks (limestone and quartzite (100 μm grain size)). The two sets of axes are related by the model ratios calculated in Table 1. (Modified from Dixon and Tirrul, 1991). The axes are related by a stress ratio of 0.0019 (model/prototype), corresponding to models deformed at 3200 g in the Queen's centrifuge, and models deformed at 160 g at the C-CORE Centrifuge. Experiments at the C-CORE centrifuge were conducted at strain rates between 10^{-3} s^{-1} and 10^{-5} s^{-1}.

References

Adam, J., Urai, J., Wienecke, B., Ooncken, O., Pfeiffer, K., Kukowski, N., Lohrmann, J., Hoth, S., V.D. Zee, W., Schmatz, J., 2005. Shear zone formation and strain distribution in granular materials – new insights employing high-resolution optical image correlation. Journal of Structural Geology 27, 283–301.

Chapman, T.J., Williams, G.D., 1984. Displacement-distance methods in the analysis of fold-thrust structures and linked fault systems. Journal of the Geological Society of London 141, 121–128.

Colletta, B., Letouzey, J., Pinedo, R., Ballard, J.F., Bale, P., 1991. Computerized X-ray tomography analysis of sandbox models; examples of thin-skinned thrust systems. Geology 19, 1063–1067.

Cooper, M.A., Trayner, P.M., 1986. Thrust-surface geometry. Journal of Structural Geology 8 (3–4), 305–312.

Coward, M.P., Potts, G.J., 1983. Complex strain patterns developed at the frontal and lateral tips to shear zones and thrust zones. Journal of Structural Geology 5, 383–399.

Cowie, P.A., Scholz, C.H., 1992. Physical explanation for the displacement-length relationship of faults using a post-yield fracture mechanics model. Journal of Structural Geology 14, 1133–1148.

Dahlstrom, C., 1970. Structural geology in the eastern margin of the Canadian Rocky Mountains. Bulletin Canadian Petroleum Geology 18, 332–406.

Davis, D., Suppe, J., Dahlen, F.A., 1983. Mechanics of fold and thrust belts and accretionary wedges. Journal of Geophysical Research 88, 1153–1172.

Dixon, J.M., Liu, S., 1992. Centrifuge modeling of the propagation of thrust faults. In: McClay, K.R. (Ed.), Thrust Tectonics. Chapman & Hall, London, pp. 53–70.

Dixon, J.M., Summers, J.M., 1985. Recent developments in centrifuge modeling of tectonic processes: equipment, model construction techniques and rheology of model materials. Journal of Structural Geology 7, 83–102.

Dixon, J.M., Summers, J.M., 1986. Another word on the rheology of silicone putty: Bingham. Journal of Structural Geology 8, 593–595.

Dixon, J.M., Tirrul, R., 1991. Centrifuge modelling of fold-thrust structures in a tripartite stratigraphic succession. Journal of Structural Geology 13, 3–20.

Eby, J.B., et al., 1923. The geology and mineral resources of Wise County and the coal-bearing portion of Scots County, Virginia. Virginia Geological Survey Bulletin 24, 617.

Eisenstadt, G., De Paor, D.G., 1987. Alternative model of thrust-fault propagation. Geology 15, 630–633.

Ellis, M.A., Dunlap, W.J., 1988. Displacement variation along thrust faults: implications fort he development of large faults. Journal of Structural Geology 10, 183–192.

Geiser, P.A., 1988. Mechanisms of thrust propagation: some examples and implications for the analysis of overthrust terranes. Journal of Structural Geology 10, 829–845.

Hubbert, M.K., 1937. Theory of scale models as applied to the study of geologic structures. Geological Society of America Bulletin 48, 1459–1520.

Jamison, W.R., 1987. Geometric analysis of fold development in overthrust terranes. Journal of Structural Geology 9, 207–219.

Jamison, W.R., 1992. Stress spaces and stress paths. Journal of Structural Geology 14, 1111–1120.

Jolley, S.J., Freeman, S.R., Barnicoat, A.C., Phillips, G.M., Knipe, R.J., Pather, A., Fox, N.P.C., Strydom, D., Birch, M.T.G., Henderson, I.H.C., Rowland, T.W., 2004. Structural controls on Witwatersand gold mineralization. Journal of Structural Geology 26, 1067–1086.

Koyi, H., Teixell, A., 1999. Where is the footwall flat? a cautionary note on template constraints. Journal of Structural Geology 21, 373–377.

Koyi, H., 1988. Experimental modeling of role of gravity and lateral shortening in Zagros mountain belt. American Association of Petroleum Geologists Bulletin 72, 1381–1394.

Koyi, H., 1995. Mode of internal deformation in model accretionary wedges. Journal of Structural Geology 17, 293–300.

Kulander, B.R., Dean, S.L., 1986. Structure and tectonics of central and southern Appalachian Valley and Ridge and Plateau provinces, West Virginia and Virginia. American Association of Petroleum Geologists Bulletin 70, 1674–1684.

Liu, S., Dixon, J.M., 1995. Localization of duplex thrust-ramps by buckling: analog and numerical modeling. Journal of Structural Geology 17, 875–886.

Liu, S., Dixon, J.M., 1990. Centrifuge modeling of thrust faulting: strain partitioning and sequence of thrusting in duplex structures. In: Knipe, R.J. (Ed.), Deformation Mechanisms, Rheology and Tectonics. Geological Society of London Special Publication, vol. 54, pp. 431–444.

Liu, S., Dixon, J.M., 1991. Centrifuge modeling of thrust faulting: structural variation along strike in fold-thrust belts. Tectonophysics 188, 39–62.

Malavieille, J., 1984. Modélisation expérimentale des chevauchements imbriqués: application aux chaînes de montagnes. Bulletin de la Société Géologique de France 7, 129–138. t. XXVI.

McClay, K., 1976. The rheology of plasticine. Tectonophysics 33, T7–T15.

McConnell, D.A., Kattenhorn, S.A., Benner, L.M., 1997. Distribution of fault slip in outcrop-scale fault-related folds, Appalachian Mountains. Journal of Structural Geology 19, 257–267.

Mitra, S., 2002. Fold accommodation faults. AAPG Bulletin 86, 671–693.

Mulugeta, G., Koyi, H.A., 1987. Three-dimensional geometry and kinematics of experimental piggyback thrusting. Geology 15, 1052–1056.

Mulugeta, G., Koyi, H.A., 1992. Episodic accretion and strain partitioning in a model sand wedge. Tectonophysics 202, 319–333.

Nicol, A., Gillespie, P.A., Childs, C., Walsh, J.J., 2002. Relay zones between mesoscopic thrust faults in layered sedimentary sequences. Journal of Structural Geology 24, 709–727.

Nicol, A., Watterson, J., Walsh, J., Childs, C., 1996. The shapes, major axis orientations and displacement patterns of fault surfaces. Journal of Structural Geology 18, 235–248.

Peltzer, G., 1988. Centrifuged experiments of continental scale tectonics in Asia. Bulletin of the Geological Institutions of Uppsala, New Series 14, 115–128.

Price, R.A., 1967. The tectonic significance of mesoscopic subfabrics in the southern Rocky Mountains of Alberta and British Columbia. Canadian Journal of Earth Sciences 4, 39–70.
Price, R.A., 1973. Large-scale gravitational flow of supracrustal rocks, Southern Canadian Rockies. In: De Jong, K.A., Scholten, R. (Eds.), Gravity and Tectonics. Wiley, New York, pp. 491–502.
Ramberg, H., 1967. Gravity, Deformation and the Earth's Crust in Theory, Experiments and Geological Applications. Academic Press, London.
Ramberg, H., 1981. Gravity, Deformation and the Earth's Crust, second ed. Academic press, p. 452.
Reks, I.J., Gray, D.R., 1983. Strain patterns and shortening in a folded thrust sheet: an example from the southern Appalachians. Tectonophysics 93, 99–128.
Storti, F., Salvini, F., McClay, K., 1997. Fault-related folding in sandbox analogue models of thrust wedges. Journal of Structural Geology 19, 583–602.
Suppe, J., Medwedeff, D.A., 1990. Geometry and kinematics of fault-propagation folding. Ecologae Geologicae Helvetiae 83 (3), 409–454.
Suppe, J., 1983. Geometry and kinematics of fault-bend folding. American Journal of Science 283, 684–771.
Teixell, A., Koyi, H., 2003. Experimental and field study of the effects of lithological contrasts on thrust-related deformation. Tectonics 22 (5), 1054–1074.
Weijermans, R., Schmeling, H., 1986. Scaling of Newtonian and non-Newtonian fluid dynamics without inertia for quantitative modeling of rock flow due to gravity (including the concept of rheological similarity). Physics of Earth and Planetary Interiors 43, 316–330.
Wibberley, C.A.J., 1997. Three-dimensional geometry, strain rates and basement deformation mechanisms of thrust-bend folding. Journal of Structural Geology 19, 535–550.
Williams, T.J., Chapman, G.D., 1983. Strains developed in the hangingwalls of thrusts due to their slip/propagation rate: a dislocation model. Journal of Structural Geology 5 (6), 563–571.
Willis, B., 1893. The mechanics of Appalachian structure. Annual Report of the US Geological Survey 13, 218–282. Part II.
Willis, L.E., Willis, 1934. Geologic Structures. McGraw Hill, New York.
Wojtal, S., Mitra, G., 1986. Strain hardening and strain softening in fault zones from foreland thrusts. Geological Society of America Bulletin 97, 674–687.
Wojtal, S., 1986. Deformation within foreland thrust sheets by populations of minor faults. Journal of Structural Geology 8, 341–360.
Woodward, N.B., 1999. Competitive macroscopic deformation processes. Journal of Structural Geology 21, 1209–1218.
Woodward, N.B., Gray, D.R., Spears, D.B., 1986. Including strain data balanced cross-sections. Journal of Structural Geology 8, 313–324.